NeuroImage 192 (2019) 156–165

Contents lists available at ScienceDirect

NeuroImage

journal homepage: www.elsevier.com/locate/neuroimage

Cortical distance, not cancellation, dominates inter-subject EEG gamma rhythm amplitude

Russell Butler [a,**], Pierre-Michel Bernier [b], Gregory W. Mierzwinski [a], Maxime Descoteaux [c], Guillaume Gilbert [d], Kevin Whittingstall [a,e,*]

[a] Department of Nuclear Medicine and Radiobiology, Faculty of Medicine and Health Science, Université de Sherbrooke, Sherbrooke, Québec, J1K 2R1, Canada
[b] Department of Kinanthropology, University of Sherbrooke, Sherbrooke, Quebec, J1K 2R1, Canada
[c] Sherbrooke Connectivity Imaging Lab, Computer Science Department, Faculty of Science, Université de Sherbrooke, Sherbrooke, J1K 2R1, Canada
[d] MR Clinical Science, Philips Healthcare Canada, 281 Hillmount Road, Markham, Ontario, L6C 2S3, Canada
[e] Department of Diagnostic Radiology, Faculty of Medicine and Health Science, Université de Sherbrooke, 12e Avenue Nord, Sherbrooke, QC, J1H 5N4, Canada

A B S T R A C T

The neurophysiological response to visual stimulation in both humans and animals is characterized by an increase in high frequency amplitude peaking in the gamma range (40–100Hz) and a suppression of low frequency amplitude peaking in the alpha range (10–16Hz). Due to the large number of studies linking amplitude and peak frequency to perception and neurological disorders, there is great interest in understanding the basis of inter-subject variability in gamma and alpha responses. To address this, we measured gamma and alpha amplitude and peak frequency of response to visual stimulation in 42 healthy humans. Using FMRI to delineate active cortical tissue in the same subjects, we correlated these neurophysiological metrics with two structural metrics: distance from active cortex to electrode, and dipole cancellation over active cortex. We find that distance strongly predicted inter-subject gamma amplitude, but had little effect on alpha amplitude, while cancellation had little effect on gamma or alpha amplitude. Neither alpha peak frequency nor gamma peak frequency correlated with our structural metrics. These results suggest that inter-subject variability in gamma amplitude may reflect gross morphology rather than neurophysiological variability, and should be interpreted with caution, while peak frequency may serve as a more sensitive metric of differences in neuronal activity across subjects.

1. Introduction

Electroencephalography (EEG) measures fluctuations in electrical potential on the surface of the scalp (Nunez and Srinivasan, 2006). These fluctuations often occur in narrowly defined frequency ranges which has led to the classification of spectrally distinct brain rhythms (Buzsáki et al., 2012) such as the alpha (10–16Hz) and gamma bands(40–100Hz). Despite the nearly 100 year history of EEG, much remains to be understood about the biophysical and anatomical basis of the brain rhythms observed from the surface of the scalp (Cohen, 2017). It is typically assumed that these rhythms arise from synaptic currents along the soma and dendrites of pyramidal cell neurons, resulting in the formation of electrical dipoles in an open field arrangement which, when the neural activity is synchronous, allows a signal to be detected on the scalp (Ahlfors et al., 2010; Irimia et al., 2012; Murakami and Okada, 2006; Musall et al., 2014). Assuming a quasi-static approximation of Maxwell's equations, dipole-based surface potentials are based on two important variables: 1) the distance and 2) the orientation of the dipole with respect to the measurement location. Consequently, the amplitude of an EEG rhythm should decrease with increasing distance and dipole cancellation (i.e. due to cortical folding) while peak frequency should be unaffected. However, while the dipole model serves as the basis for a large body of literature attempting to relate scalp potentials to cortical activity (Buzsáki et al., 2012; Gramfort et al., 2010), to date no study has empirically examined the degree to which these variables (distance and orientation) affect inter-individual differences in human brain activity. Might certain individuals with more tightly folded cortices, or cortices further from the scalp exhibit different EEG spectral signatures? Simulation studies have shown that cortical depth and not orientation is the main factor comprising sensitivity of MEG (Hillebrand and Barnes, 2002), but how these findings generalize to frequency specific EEG signals is unknown. In theory, cancellation due to simultaneously active, oppositely oriented dipoles has a strong effect on both MEG and EEG (Ahlfors et al., 2010; Lin et al., n.d.) but to our knowledge this has not been investigated empirically to date.

Many studies have reported that visually induced EEG responses in

* Corresponding author. Department of Diagnostic Radiology, Faculty of Medicine and Health Science, Université de Sherbrooke, 12e Avenue Nord, Sherbrooke, QC, J1H 5N4, Canada.
** Corresponding author.
E-mail addresses: Russell.Buttler@usherbrooke.ca (R. Butler), kevin.whittingstall@usherbrooke.ca (K. Whittingstall).

https://doi.org/10.1016/j.neuroimage.2019.03.010
Received 9 January 2019; Accepted 5 March 2019
Available online 9 March 2019

aging or neurologically impaired populations is significantly altered (Coppola et al., 2007; Dickinson et al., 2016, 2015; Peiker et al., 2015; Simon and Wallace, 2016; Spencer et al., 2008; Sun et al., 2012; Tan et al., 2013). Since many of these patients also show morphological alterations in brain structure, it is possible that these structural differences are the main driver behind the appearance of 'abnormal' activity measured at the scalp. This is supported by the fact that inter-subject variability in healthy subjects is large despite the gamma rhythm's stability within individuals across both hours and days (Muthukumaraswamy et al., 2010) as well as in identical twins which points to a strong genetic basis for inter-individual differences in the gamma peak frequency (van Pelt et al., 2012). Some studies have investigated the role of factors such as the surface area, thickness, volume and GABA concentration in primary visual cortex (V1) with mixed results (Cousijn et al., 2014; Kujala et al., 2015; Muthukumaraswamy et al., 2009; Provencher et al., 2016; Robson et al., 2015; Schwarzkopf et al., 2012). No study, to our knowledge, has directly quantified the role of dipole distance and cortical cancellation, which could be major determinants of the EEG scalp potential.

To address this, we employed a multi-modal imaging approach, using FMRI to localize subject specific activations, structural MRI to obtain cortical and head morphology, and EEG to measure the neurophysiological response. We then compared our subject specific FMRI-constrained morphology metrics with EEG responses in the same group of healthy humans. Based on the traditional mechanisms underlying the dipole model, we hypothesized that gamma and alpha amplitude would be equally (inversely) correlated to distance and cortical cancellation, whereas peak frequency would be unaffected by these structural metrics. We should note that in our cancellation index, we considered only cancellation amongst dipoles normal to the cortical surface, we did not consider the dipole orientation relative to the electrode, therefore these results should generalize to both EEG and MEG despite the fact that these two modalities are more sensitive to radial and tangential dipoles respectively (Cohen et al., 1990).

2. Methods

Subjects: Informed consent was obtained according to the guidelines of the Internal Review Board of the Centre Hospitalier Universitaire de Sherbrooke. A total of 42 subjects were acquired, (n = 24 in group 1, n = 8 in group 2, n = 10 in group 3) over three separate experimental paradigms; groups 1&3 were acquired during separate EEG and FMRI sessions, while group 2 was acquired during a simultaneous EEG-FMRI session. No psychiatric or neurologic symptoms were present in any subjects at the time of scanning or in the past, and all subjects had normal or corrected to normal vision.

Stimulus construction and presentation: All stimuli were generated and presented using Psychophysics Toolbox (BRAINARD, 1997). Subjects were required to fixate on a central crosshair for the duration of the experiment. For group 1, all stimuli were variations of a drifting sinusoidal grating with the following parameters: spatial frequency 3 cycles/degree, temporal frequency 6 cycles/second, drifting from right to left within a 7-degree circular aperture in the centre of the subject's visual field. Six separate grating patterns (Fig. 1A) were used to induce a wide range of gamma responses (Hermes et al., 2015a, 2015b): 1) 100% contrast (described above), 2) 10% random, 3) 60% random, 4) plaid, 5) 33% contrast, and 6) 5% contrast. Further details on stimulus construction are also available in a previous publication (Butler et al., 2017a). For group 2, stimuli were full field (Fig. 1B) and grating patterns were 1) 0% random (equivalent to 100% contrast), 2) 10% random, and 3) 100% random. For group 3, stimuli were full field, 100% contrast gratings (Fig. 1C), and instead of drifting from right to left, were rotated around the fixation point in either clockwise or counter-clockwise directions, at 2.6°/second. Group 1 EEG signals were acquired outside the scanner with stimuli presented on a CRT monitor (800x600 pixels, frame rate = 85Hz) at a rate of 1 stimulus every 5 s (2 s stimulus duration, 3 s ISI), each of the 6 stimulus types was presented 135 times (810 trials per subject). For group 2 simultaneous EEG-FMRI experiment within the scanner stimuli were projected from an MRI-compatible monitor (800x600 pixels, frame rate 75Hz) to a mirror positioned above the subject's face attached to the head coil, at a rate of 1 stimulus every 10 s (5 s stimulus duration, 5 s ISI) for a total of 96 trials (32 trials/stimulus type). Group 3 EEG was acquired with the same setup as group 1 (outside the scanner), but with a stimulus duration of 18 s (for one full grating rotation), an ISI of 5 s, and 15 trials/stimulus type. Group 1&3 visual FMRI experiments were conducted in the same scanner setup as group 2, but with 45 trials/stimulus type (270 trials per subject), 2 s stimulus duration and 14 s ISI (group 1) (Fig. 1D), and an alternating 10 s on/off visual grating block design over the course of 8 min (group 3).

2.1. MRI acquisition and preprocessing

Acquisition: Whole brain BOLD FMRI volumes were acquired on a 3T MRI scanner (Ingenia, Philips Healthcare) using a 32 channel head coil for reception. The FMRI sequence differed slightly between groups. Group 1 (n = 24) sequence parameters: TR/TE = 2000/30 ms, flip angle = 70°, FOV = 224x224 × 136.5 mm, voxel size = 3.5 mm isotropic, no multiband acceleration. Group 2 (n = 8) sequence parameters: TR/TE = 693/30 ms, flip angle = 50°, FOV = 240 × 240 × 123.75 mm, voxel size = 3.75 mm isotropic, multiband acceleration factor 3. Group 3 (n = 10) sequence parameters: TR/TE = 680/30 ms, flip angle = 52°, FOV = 240x240 × 126mm, voxel size = 3 mm isotropic, multiband acceleration factor = 6. An anatomical T1-weighted 3D gradient-echo image (TR/TE = 7.9/3.5 ms, flip angle = 8°, FOV = 240x240 × 150mm, voxel size = 1 mm isotropic) was acquired following FMRI acquisition sessions for all groups.

2.2. EEG recording and preprocessing

Groups 1&3 (n=24, n=10, non-simultaneous acquisition) EEG recording: Scalp signals were acquired on a 64 channel EEG actiCap system (Brain Products) sampling at 500Hz referenced from electrode Fz according to the 10–20 system. The experimenter positioned the cap according to the following anatomical landmarks: electrode Oz directly superior to the inion, and the midpoint between electrodes Cz and reference on the apex of the head. **Preprocessing:** Poorly connected electrodes were isolated using visual inspection of the raw electrode time series, and interpolated using spherical interpolation (Delorme and Makeig, 2004). To maximize the signal to noise ratio (SNR) of the EEG response, temporal independent component analysis (ICA) (Delorme and Makeig, 2004) was performed on each subject separately after applying a 1–120Hz bandpass filter, resulting in 64 components per subject. To isolate ICA components of neural activity in visual cortex and remove ICA components of ocular/muscular/-other origin, the following procedure was applied: First, a neuronal response function (NRF) was defined by hand-picking in each subject the top ICA component whose event-related spectral perturbation (ERSP) most strongly resembled narrow band gamma and alpha induced activity seen in previous macaque and human studies (Fries et al., 2008). This component's scalp weight map always resembled a dipole restricted to posterior channels. Upon selecting this single component in each subject, the ERSP from this component was averaged across all subjects, to form a "template" NRF. The NRF was then averaged across both gamma (40–100Hz) and alpha (10-16HZ) to form two separate time series. These two separate time series from the NRF were then correlated with single trial alpha and gamma time series amplitude respectively, from each ICA component separately, and components were sorted according to their mean single trial correlation to the NRF (after averaging the alpha and gamma correlations together). Correlations with the NRF were performed on a single trial basis and then averaged in order to filter out bad components with large, broadband gamma activity in a few trials due to

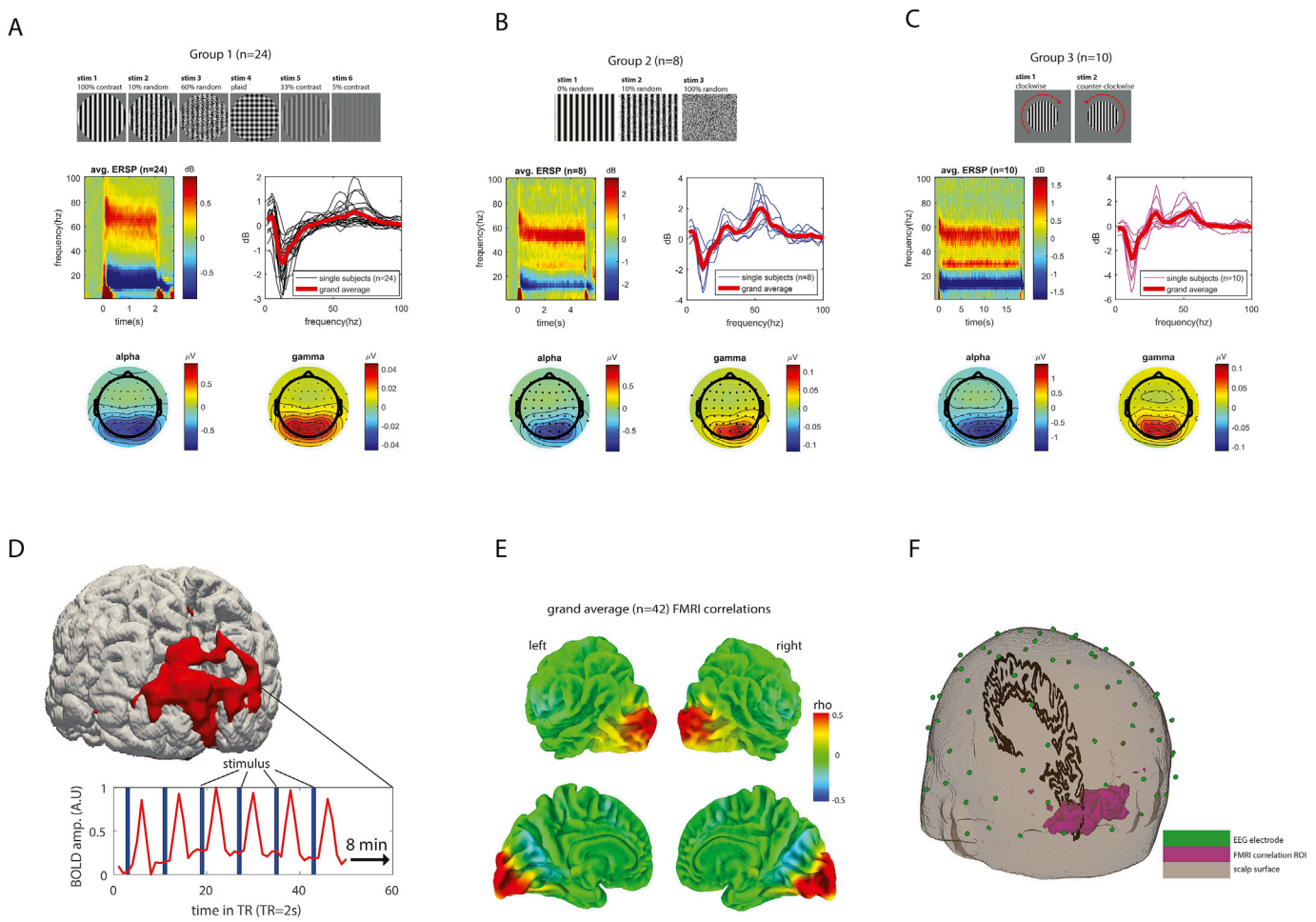

Fig. 1. A) Group 1 stimuli (top), group average event-related spectral perturbation (ERSP) in units of decibels (dB) (middle left), single subjects and group average across time (middle right), and group average scalp topography in units of micro-volts for stimulus induced alpha changes (task minus baseline) (bottom left) and gamma changes (bottom right).

B) Same as (A), but for group 2 (n = 8) which was acquired during a simultaneous EEG-FMRI session.

C) Same as (A) but for group 3 (n = 10). Stimulus was a more prolonged (18 s trials) rotating high contrast grating, either clockwise (stim 1) or counter-clockwise (stim 2).

D) Schematic showing how the functional magnetic resonance (FMRI) region of interest (ROI) was obtained in a single subject – stimulus design time series (blue bars) was convolved with a canonical hemodynamic response function (HRF) and correlated with BOLD time series (red trace) in each voxel, correlation maps were then thresholded to yield a binary ROI in each subject (red overlay).

E) Grand average FMRI ROI across all subjects (n = 42) showing left/right hemispheres from the lateral (top) and medial (bottom) view.

F) Schematic showing electrode locations (green) relative to the FMRI ROI (purple) in a single subject. Distance was defined at each electrode as the Euclidean distance between the electrode location and the center of mass of FMRI ROI in either hemisphere. See Supplementary 1D for analysis of distance obtained using precise electrode coordinates from the UTE image obtained during the simultaneous EEG-FMRI experiment vs distance obtained using average electrode coordinates mapped from the MNI template.

muscle or jaw movements (Muthukumaraswamy, 2013). Upon sorting each subject's 64 components according to NRF correlation, the top 5 components in each subject were selected for further analysis and projected back to channel level. On average, selecting for the top 5 neural components in each subject retained ~25% of the variance relative to the raw data.

Group 2 (n=8) EEG recording: Scalp signals were acquired on a 64 channel MR-compatible EEG cap (Brain Products) sampling at 5000Hz (high sampling rate in order to later remove MRI induced gradient artifacts) referenced from electrode Fz according to the 10–20 system. The cap was positioned according to the same anatomical landmarks as in Groups 1&3, by the same experimenter, and electrodes were later precisely localized inside the scanner using an ultra-short echo time (UTE) sequence (Butler et al., 2017b) which is capable of directly imaging the plastic materials of the EEG cap. Preprocessing was identical to that described for Groups 1&3.

2.3. Analysis

Alpha and gamma amplitude: After ICA denoising and back projection to channel level, EEG amplitude was defined at each channel separately for each subject and stimulus type by the following procedure: scalp signals were filtered into 2 separate bands, 1) alpha (10–16Hz) and 2) gamma (40–100Hz) and rectified (Hari and Salmelin, 1997). Each band was then epoched according to stimulus onset, and amplitude (in units of micro-volts) was defined at each electrode and each band by subtracting mean of baseline (−1 to 0 s) from mean of stimulus duration (2 s for group 1, 5 s for group 2, 18 s for group 3) and then averaging across trials. A single gamma and alpha amplitude value was obtained for each subject by averaging amplitude over all posterior electrodes (Fig. 1A, B, 1C) and stimulus types. Left/right hemisphere amplitude values were also obtained by averaging across left/right electrodes respectively.

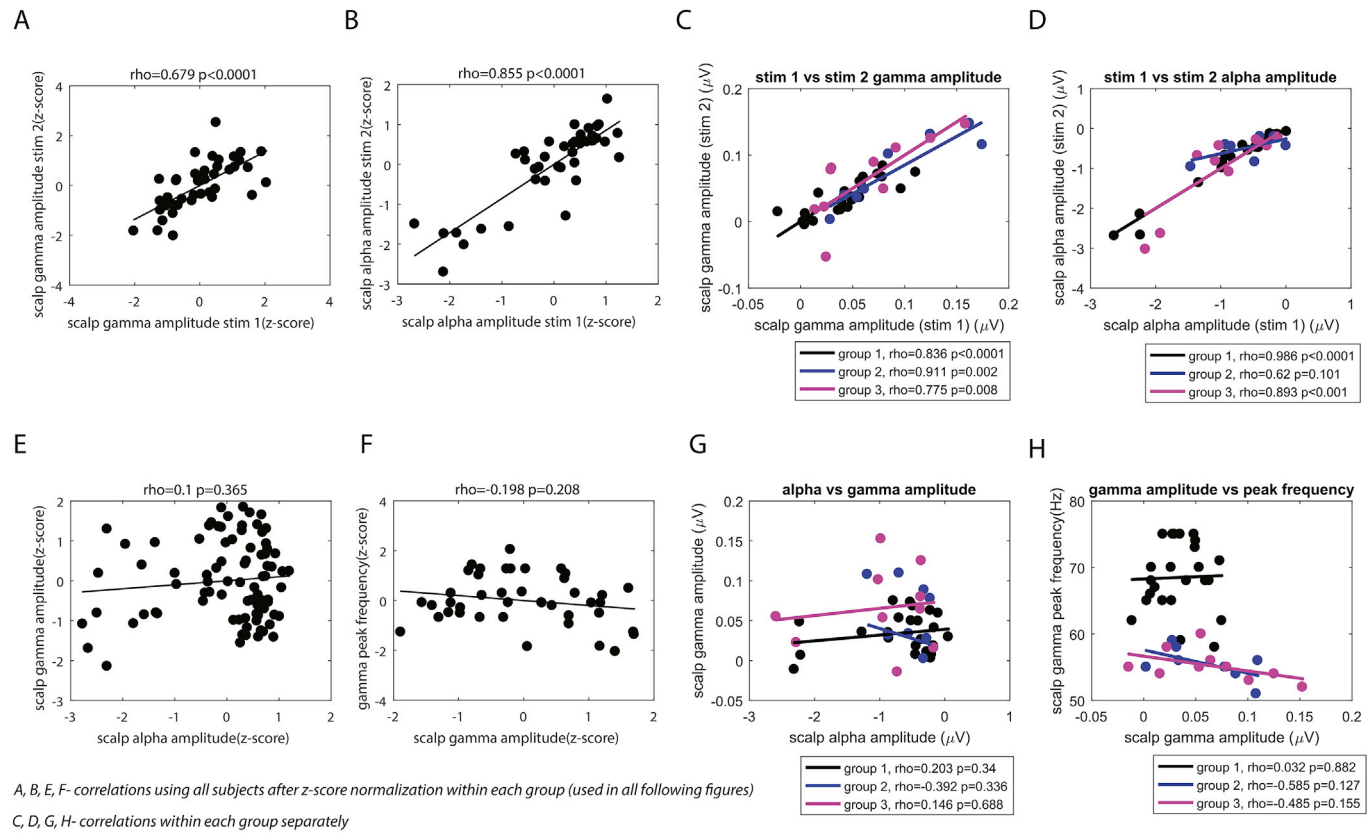

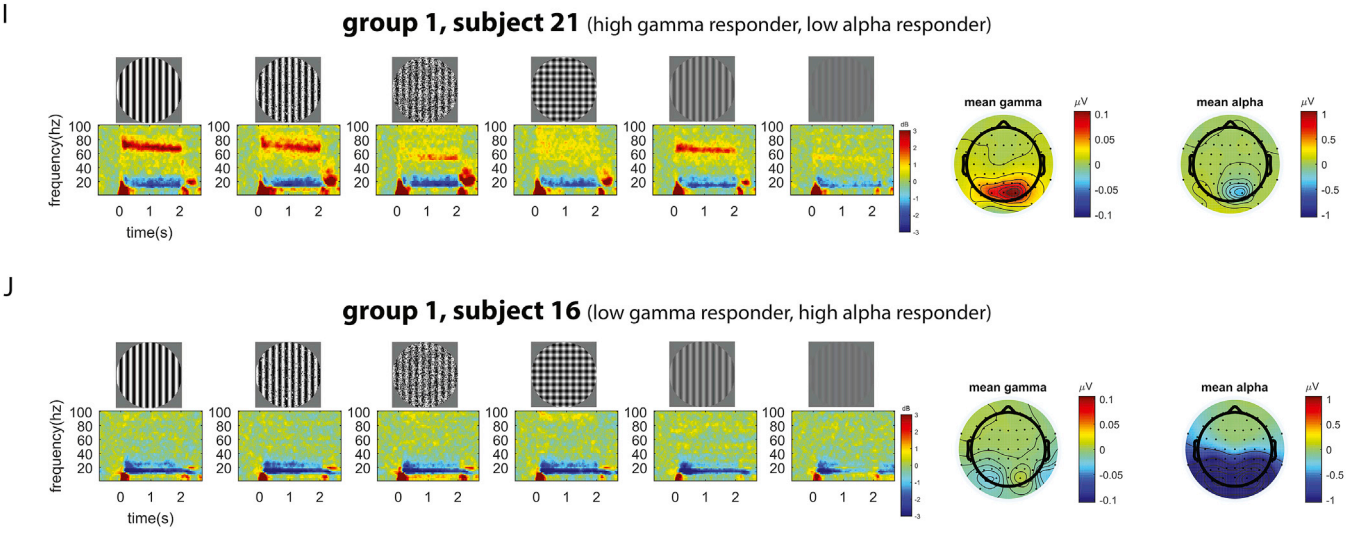

Fig. 2. A) Inter-stimulus scalp gamma amplitude correlation across all subjects (pooled using z-score method). Subjects who responded strongly to stimulus 1 also responded strongly to stimulus 2 (see Fig. 1 for definition of stimulus 1&2 in the separate groups).
B) Same as (A) but for scalp alpha amplitude.
C) Same as (A), but correlations were computed across each group separately, using the raw micro-volt values obtained on the scalp.
D) Same as (C), but for scalp alpha amplitude.
E) Gamma vs alpha amplitude correlation across all subjects (pooled using z-score method). Strong alpha band responders were not necessarily strong gamma band responders.
F) Gamma amplitude vs gamma peak frequency correlation across all subjects. No consistent relationship between gamma amplitude and peak frequency.
G) Same as (E), but correlations computed across each group separately using raw micro-volt values obtained at the scalp.
H) Same as (F) but correlations computed across each group separately using raw micro-volt values.
I) Subject 21 from group 1 ERSP
response to all stimuli (see Supplementary 1 for all subjects). This subject responded strongly to all stimuli in the gamma range, and only moderately in the alpha range. J) Same as (I) but for subject 16. This subject responded poorly to all stimuli in the gamma range, and strongly in the alpha range.

Gamma peak frequency: Gamma peak frequency was defined at the ICA component level rather than the channel level (Muthukumaraswamy et al., 2009; Schwarzkopf et al., 2012). Event-related spectral perturbation (ERSP) (Fig. 1A, B, 1C, Supplementary 1A, 1B, 1C) was computed on the ICA component time series by computing log power in partially overlapping 250 ms Hanning windows (Delorme and Makeig, 2004) at 200 equally spaced time points for each ICA gamma component, then subtracting the baseline (−1000 ms–0 ms) to yield a decibel (dB) value at each time-frequency bin. For each subject, the ERSP was then averaged across ICA components (5 per subject), stimulus types, and stimulus duration. The initial 500 ms was not included in peak frequency estimation to avoid stimulus onset effects, ensuring that these measurements include only the peak during the sustained narrow-band gamma response. The gamma peak frequency for each subject was then defined simply as the frequency band between 40Hz and 100Hz with the highest amplitude.

FMRI regions of interest: An FMRI region of interest (ROI) was defined in each subject separately by convolving the stimulus design time series with a hemodynamic response function (HRF) (Friston et al., 1994) and correlating the HRF-convolved time series with the FMRI signal in each voxel (Fig. 1D). Correlation maps were then aligned to each subject's anatomical T1 (1 mm isotropic) (Jenkinson et al., 2012), where all subsequent analysis was performed (Fig. 1E). Binary regions of interest (ROIs) were defined in each subject by sorting the correlation values from highest to lowest, and setting the top 10000 correlated voxels to one, and all other voxels to zero (in T1 space, where each voxel was 1 mm isotropic) – this procedure resulted in the same ROI volume in each subject. This ensures that each subject's activation center of mass approximation was based on the same volume ROI.

Distance from active cortex to electrode: distance was defined at each electrode as the Euclidean distance from the three-dimensional center of mass of each subject's visually induced FMRI ROI to the electrode location (Fig. 1F). To obtain a single distance measure in each subject, distance values between electrode and FMRI ROI center of mass were averaged across all posterior electrodes (P, PO, and O). Separate left/right hemisphere to left/right occipital electrode distances were also obtained in each subject, by masking the FMRI ROI with left/right hemisphere gray matter masks obtained from Freesurfer, and repeating the above procedure. In group 2, distances were accurate to within 1 mm (Butler et al., 2017b) as the electrodes were imaged directly within the scanner using a UTE MRI sequence. In groups 1&3, locations were not measured directly but instead obtained by the following procedure: UTE localized coordinates from each subject in group 2 were mapped to the MNI152 anatomical template (Evans et al., 2012) based on a 12 DOF affine transform from each subject's T1 (Jenkinson et al., 2012). Group 2 coordinates were then averaged across all subjects in MNI space, to create an average electrode coordinate template in the MNI152. The electrode coordinate template was then mapped to each subject in groups 1&3, again using a 12 DOF affine transform based on the T1 (Supplementary 1D). Correlating the distance from electrode to FMRI ROI obtained using the ground truth (UTE) and atlas-based (MNI152) coordinates revealed that the atlas-based coordinates were an excellent approximation of the true electrode to FMRI ROI distance (Supplementary 1E).

Skull/scalp distance: distance from active cortex to electrode was divided into two segments based on anatomical boundaries 1) the distance from FMRI ROI center of mass in each hemisphere to the inner skull boundary and 2) the distance from the inner skull boundary to the outer scalp tissue directly beneath the electrode. The inner skull and outer scalp boundaries were obtained using FSL's BET command (Jenkinson et al., 2012) with each subject's T1 image as input. A schematic illustrating these distances is provided in Fig. 3A (created using the Fibernavigator visualization software) (Chamberland et al., 2015).

Cancellation Index: The cancellation index (I_0) was defined as in Irimia et al. (2012) with increasing values of I_0 indicating greater cancellation of normal surface vectors. Normal vectors were obtained by intersecting the Freesurfer white matter surface normals with each subject's FMRI ROI mask. Briefly, cancellation was computed by summing the normal vectors across the FMRI ROI into a single vector and then summing the magnitude of this vector's x, y, and z components, and subtracting this value from 1, details in (Irimia et al., 2012). Higher values of I_0 indicate greater cancellation. Also, as I_0 increases systematically with the number of normal vectors used in the calculation, we constrained the number of normal vectors to be the same in each subject (top 2000 normal vectors with highest activation) and we obtained similar results when using a range of normal vectors across the entire FMRI ROI (see Supplementary 2F).

Source Localization: EEG Source-localization was carried out using the Brainstorm software (Tadel et al., 2011). The minimum norm source estimate (MNE) technique was used. Sources were modelled as unconstrained dipoles (with identity noise) within a 3 shell spherical head model based on subject specific T1 images, and reconstructed to a 8 mm^3 grid. The source time-series was epoched and the same procedure used to obtain alpha and gamma amplitude at the electrode level was applied to each source voxel to obtain source amplitude estimates. The source grid was aligned and up-sampled to the anatomical T1 for visualization and analysis of source and FMRI activation overlap. Source amplitude was defined in each subject as the mean task-baseline (see alpha and gamma amplitude above) across the 10000 up-sampled (1 mm isotropic) source voxels with highest amplitude difference from task to baseline.

Pooling of subjects and hemispheres: Subjects from all 3 groups were pooled into a single group by z-score normalization of gamma amplitude and structural metrics within each group separately. This was done to generalize our results across all subjects in addition to reporting correlation values in each separate group (see Supplementary 2). Furthermore, distance and cancellation were computed for each hemisphere (left/right) separately, and compared to scalp gamma amplitude in left/right electrodes separately effectively doubling the number of points in each scatter plot from $n = 42$ to $n = 84$. This provided more realistic distance and cancellation (I_0) estimates, as the center of mass of FMRI ROI was pulled towards the midline when using both hemispheres together to compute center of mass. When considering the two hemispheres separately the center of mass for left/right hemisphere FMRI ROI was in gray matter, as expected. Regardless of the exact method for computing center of mass (two hemispheres separately, or both hemispheres together) or pooling of subjects (correlating across the 3 groups separately, or pooling all subjects using z-scores) similar results were achieved (Supplementary 2). All correlations, unless otherwise specified, were carried out using Spearman's Rho.

3. Results

Narrow band gamma (NBG) is observable in all 3 groups: Despite the wide range of grating parameters used, grand average stimulus-induced changes for groups 1, 2, and 3 revealed a strong gamma peak in all groups (Fig. 1A, B, 1C) along with significant inter-subject variability in both gamma and alpha frequency bands. Scalp maps revealed stimulus induced gamma and alpha changes restricted to occipital and parietal electrodes overlying visual cortex (Fig. 1A, B, 1C). Grand average ($n = 42$) FMRI correlation map revealed that activity from all stimuli was constrained to the primary visual areas of the occipital pole (Fig. 1E).

Inter-subject EEG amplitude is consistent across stimulus types: Subjects who were high amplitude responders to stimulus 1 (high contrast drifting grating for group 1&2, clockwise rotating grating for group 3) also responded strongly to stimulus 2 (randomized gratings for group 1&2, or counter-clockwise rotating grating for group 3) in both the gamma range (Fig. 2A, $rho = 0.68$, $p < 0.0001$) and alpha range (Fig. 2B, $rho = 0.86$, $p < 0.0001$), justifying the pooling across stimulus types when comparing EEG amplitude with anatomical structure. The same effect was observed when computing the correlations using raw micro-volt values across each group separately (Fig. 2C and D). However, subjects with strong alpha responses were not necessarily strong gamma responders to the same stimulus (Fig. 2E, $p = 0.365$, see separate groups in

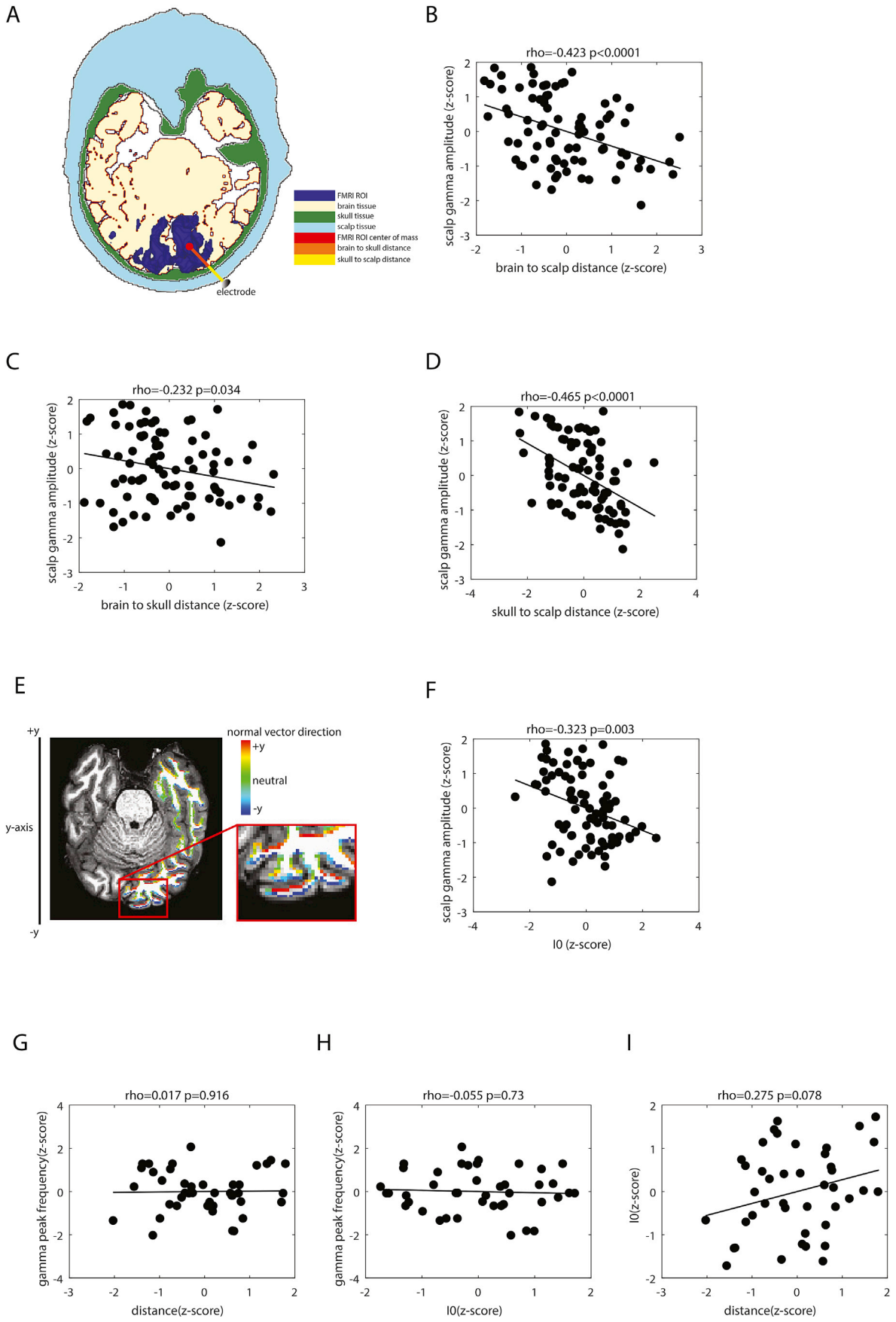

(caption on next page)

Fig. 3. A) Schematic showing the different distance metrics used, based on the FMRI ROI center of mass (right hemisphere only) as starting point. As noted in methods, brain (which refers to the FMRI ROI center of mass) to scalp electrode distance was split into two parts 1) brain to inner skull and 2) inner skull to scalp.
B) Brain to scalp (electrode) distance vs scalp gamma amplitude (pooled across all subjects and both hemispheres using the z-score method, for a total of 84 data points – 42 subjects, 2 hemispheres/subject). Mean gamma amplitude over left/right electrodes was matched with mean distance from those electrodes to left/right hemisphere FMRI ROI center of mass respectively.
C) Brain to inner skull distance vs scalp gamma amplitude (pooled as in (B)). The brain to inner skull distance is composed of a mix of gray/white matter and cerebrospinal fluid (CSF).
D) Inner skull to scalp distance vs scalp gamma amplitude (pooled as in (B)). The inner skull to scalp distance is composed of a mix of bone, skin, and fat.
E) Schematic from a single subject showing how cortical cancellation (I_0) was defined. The y-component of the white matter normal vectors is shown here (x and z components not shown), blue implies the normal vector points from anterior to posterior direction, red implies the normal vector points from posterior to anterior direction, green implies it has no preference in the y-direction.
F) Cortical cancellation (I_0) vs gamma amplitude measured at the scalp. I_0 was computed in left/right hemisphere separately for each subject, and matched to gamma amplitude averaged across left/right occipital electrodes in that subject.
G) Distance (averaged across both hemispheres) vs gamma peak frequency (a single gamma peak frequency was defined in each subject, rather than a separate peak frequency for each hemisphere).
H) Same as (G) but for I_0 vs gamma peak frequency. I) Distance (averaged across both hemispheres) vs I_0 (averaged across both hemispheres).

Fig. 2G). Gamma peak frequency was not correlated with gamma amplitude (Fig. 2F, $p = 0.21$, see separate groups in Fig. 2H). An example ERSP from two subjects is shown in Fig. 2I and J: note how subject 21 is a relatively strong gamma and weak alpha responder while subject 16 is a strong alpha, weak gamma responder.

Distance predicts gamma but not alpha amplitude across subjects: The above results suggest that there may exist a common anatomical factor underlying EEG amplitude variability in healthy subjects. We first examined the effects of distance (Fig. 3A). Pooling all subjects and hemispheres and correlating distance with gamma amplitude revealed a highly significant inverse relationship (Fig. 3B, $rho = -0.42$, $p < 0.0001$), however distance did not explain inter-subject alpha amplitude variability (Supplementary 2A, $p = 0.27$). To ensure this result was not driven by potential biases in our FMRI ROI estimate, and investigate the contribution of different tissue types to the distance correlation, we further separated the distance into two components: 1) brain to skull distance (Figs. 3C) and 2) skull to scalp distance (Fig. 3D). While both components showed a significant inverse relationship with gamma amplitude, it was skull to scalp distance ($rho = -0.47$, $p < 0.0001$) that correlated best. Alpha amplitude did not correlate with brain to skull (Supplementary 2A, $p = 0.82$) or skull to scalp (Supplementary 2A, $p = 0.3$). The distance vs gamma/alpha correlations for each group and hemisphere separately are similar to the pooled results, and are shown in supplementary 2B-C.

Cancellation is a poorer predictor of gamma amplitude than distance: Correlating the cancellation index (I_0) (Fig. 3E) with amplitude revealed a weak but significant inverse relationship with scalp gamma amplitude (Fig. 3F, $rho = -0.32$, $p = 0.003$) and no relationship to scalp alpha amplitude (Supplementary 2E, $p = 0.95$). I_0 vs gamma/alpha amplitude correlations for each group separately were similar to the pooled results, shown in supplementary 2E. We also examined the I_0 vs EEG amplitude correlation as a function of frequency from 1 to 100Hz, and as a function of the number of normal vectors considered in the I_0 computation, showing a trend for positive I_0 vs EEG correlations in the lower frequencies (10–20Hz) and an inverse correlation in the higher frequencies (40 + Hz) (Supplementary 2F, uncorrected p-values).

Peak Frequency does not correlate with distance or cancellation: Neither distance (Fig. 3G, $p = 0.92$) nor I_0 (Fig. 3F, $p = 0.73$) correlated with gamma peak frequency, and results were similar when considering the 3 groups separately (Supplementary 2G).

I_0 and distance are only loosely correlated: Subjects with larger FMRI ROI to electrode distances did not necessarily exhibit higher I_0 (Fig. 3G, $rho = 0.27$, $p = 0.08$), indicating that our anatomical metrics (I_0 and distance) were independent of one another.

Sex differences in anatomy but not FMRI correlation strength recapitulate sex differences in gamma amplitude: A significant sex difference in scalp EEG gamma amplitude was observed, with females exhibiting higher amplitude (Fig. 4A, $p = 0.013$). This sex difference was recapitulated by differences in distance, with females exhibiting significantly shorter distances from FMRI ROI to electrode (Fig. 4B, $p < 0.001$), and to a lesser extent I_0 (Fig. 4C, $p = 0.024$) but not functional (FMRI) correlation strength (Fig. 4D, $p = 0.424$). Sex difference analysis was restricted to the larger group (group 1, $n = 24$) due to the fact that the groups were not perfectly balanced according to sex, and different stimuli were used for each group, but similar results were obtained when pooling across all subjects using z-scores (data not shown).

Effects of source localization on sex differences and distance correlation: MNE source estimates based on a 3-shell sphere (Fig. 4E) revealed a strong, significant correlation between scalp gamma amplitude and source gamma amplitude (Fig. 4F, $rho = 0.86$, $p < 0.0001$). However, the distance vs gamma amplitude correlation was attenuated at the source level (Fig. 4G) ($p = 0.005$ at the source level vs $p < 0.0001$ at the scalp level), and sex differences in gamma amplitude were also reduced at the source level (Fig. 4H) ($p = 0.04$ at the source level, $p = 0.01$ at the scalp level).

4. Discussion

The objective of this study was to determine the extent to which variability in gross head/brain morphology across subjects predicts variability in neurophysiological responses to visual stimulation measured using EEG. Previous works have focused on morphological metrics such as cortical thickness (Provencher et al., 2016; van Pelt et al., 2018), surface area (Schwarzkopf et al., 2012), or neurochemical metrics such as GABA concentration (Kujala et al., 2015; Muthukumaraswamy et al., 2009), and simulation studies have investigated the effects of source distance and orientation (Hillebrand and Barnes, 2002) on MEG signals, while our study is the first to empirically examine the effects of distance and cancellation on experimental human EEG signals.

In our first set of results (Fig. 1, Supplementary 1) we show that while on average our grating stimuli elicit strong narrow band alpha and gamma responses in all 3 groups, there is a great deal of inter-subject variability, especially in the gamma range. Interestingly, subjects who responded strongly to one type of stimulus also responded strongly to other stimuli, in both alpha and gamma range. However, there was no consistent relationship between alpha and gamma scalp amplitude (strong alpha responders were not necessarily strong gamma responders), and a similar result has been reported in 97 MEG subjects (Shaw et al., 2017).

The scalp potential equation governing EEG signal amplitude (Nunez and Srinivasan, 2006) contains two variables that we were able to approximate using our methods: distance (approximated using Euclidean distance from FMRIROI centroid to electrode) and dipole angle (approximated using cancellation index I_0). We noted an inverse correlation between distance and gamma amplitude; subjects with shorter distances were also higher amplitude gamma responders. This shows that differences in non-invasively measured gamma amplitude across subjects, while perhaps related to differences in recurrent and intrinsic

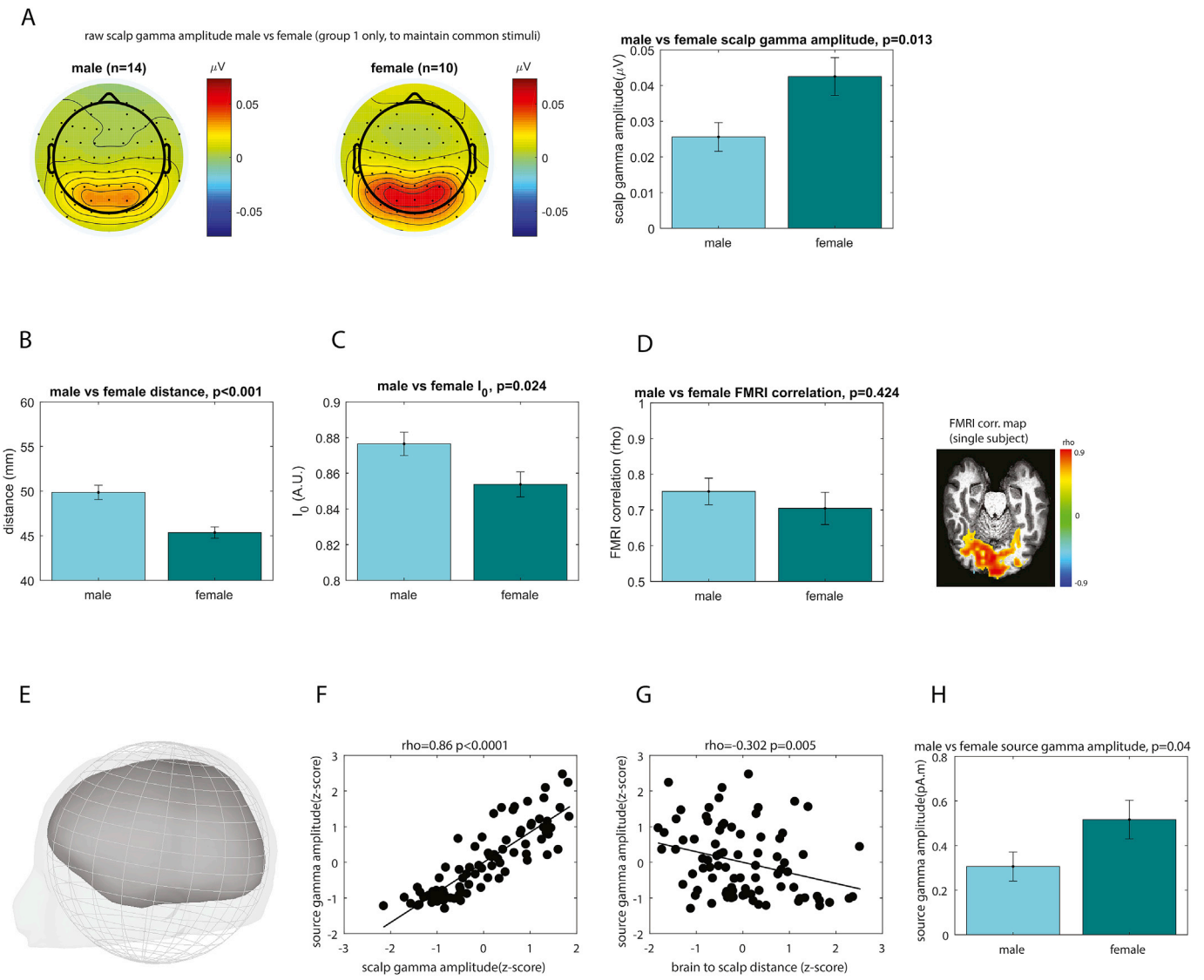

Fig. 4. A) Male vs female scalp gamma amplitude. Group 1 only was used for the sex difference comparison, as the number of male/female in each group was not perfectly balanced, and the groups used different stimuli.
B) Male vs female distance (Group 1 only).
C) Same as (B) but for I_0.
D) Same as (B) but for FMRI correlation strength (defined as the mean correlation coefficient within the binary FMRI ROI).
E) Schematic showing the outer sphere and brain surface used in the 3-shell sphere MNE source modeling (Brainstorm).
F) Source gamma amplitude vs scalp gamma amplitude (pooled across all subjects (n = 42) and hemispheres (2) using z-score method).
G) Distance vs source gamma amplitude (pooled across all subjects (n = 42) and hemispheres (2) using z-score method). H) Male vs female source gamma amplitude (Group 1 only (n = 24, 14 male, 10 female)).

connections between pyramidal and inhibitory cells (Shaw et al., 2017), are also driven by additional measures such as Euclidean distance between cortex and scalp. Interestingly, this distance relationship was not present in the alpha band. We attribute this to two possible factors 1) alpha amplitude was an order of magnitude higher than gamma amplitude. Background noise due to changes in impedance or muscular activity may thus be relatively higher in the gamma range, and small changes in distance would have a stronger effect on gamma signal to noise ratio (SNR) than alpha SNR, therefore gamma would be more sensitive to distance than alpha. This may also explain why some subjects were non-responders in the gamma range, but responded in the alpha range. Alternatively, 2) alpha and gamma in response to our task may originate from different areas, and the FMRI ROI may be a better representation of local gamma activity. While gamma has been linked to feedforward neural activity (Bastos et al., 2014) which is tightly co-localized to blood oxygen level dependent FMRI (Goense and Logothetis, 2008), the spatial origin of our alpha responses remains less well understood and may not match the centroid of FMRI activation as closely as gamma. Source amplitude was also found to be dependent on distance (Fig. 4G), although the effect was much weaker than the correlation between sensor level (scalp) gamma amplitude and distance. This suggests that source localization may help to mitigate the effects of distance on inter-subject gamma amplitude.

It may seem puzzling that while the electric potential of a dipole falls off due to distance according to the inverse-squared law (Nunez and Srinivasan, 2006), our inter-subject distance vs gamma relationship was linear (Fig. 3A, B, 3C). However, the inter-subject distance range was only 40–60 mm, on average (Supplementary 2B-C). The linear shape of

the distance vs gamma correlation can therefore likely be attributed to the relatively narrow range of distances across subjects when examining posterior electrodes only.

In addition to distance, we also quantified the extent to which the cancellation index (I_0) was correlated to both alpha and gamma amplitude across subjects. I_0 had a much weaker effect on gamma amplitude than distance. This finding was unexpected given the long-held belief that the relative orientation of dipoles perpendicular to the cortical surface strongly affects EEG signal strength due to dipole cancellation (Ahlfors et al., 2010; Irimia et al., 2012). The source of this result is unclear, but could be due to the following: First, recent experimental and theoretical studies have reported that monopoles make an unexpectedly strong contribution to extracellular voltage measurements (Destexhe and Bedard, 2012; Riera et al., 2012) which would suggest that cortical orientation may not play as big a role as expected. Second, the variability in I_0 across our subjects was relatively small (~5%) compared to ISV_{GA} (~100%). Finally, despite the fact that we computed cancellation in each hemispheres separately, I_0 remains a global curvature metric that does not take into account the distance between opposing dipoles. It is unreasonable to expect dipoles 20 mm apart to cancel equally with dipoles 2 mm apart, although the I_0 calculation makes this assumption. A different cancellation metric which takes into account the distance between opposing dipoles may yield a better prediction of EEG amplitude. Nevertheless, our results are in line with simulation studies (Whittingstall et al., 2003) showing that source depth – not orientation – is the main determinant of the surface EEG signal.

Peak frequency was unrelated to any of the structural parameters (distance, cancellation). This result is unsurprising, as invasive studies have also found no consistent relationship between peak frequency and amplitude in non-human primate responses to similar stimuli (Jia et al., 2013). This provides further evidence that peak frequency is independent of macroscopic anatomical brain features and hence may serve as a more easily interpreted biomarker of functional processing in studies of neurodegeneration, cognitive disorders, or perceptual processing. Alternatively, metrics new metrics which track EEG signal propagation along white matter pathways (Deslauriers-Gauthier et al., 2017) could also be of use.

Contrary to a previous study investigating sex differences in gamma amplitude using MEG (van Pelt et al., 2018), we found significant sex differences in our scalp EEG measurements, with females exhibiting higher amplitude scalp gamma than males. The disparity between our EEG results and the MEG results of Van Pelt et al. may be due to the fact that, while both magnetic and electrical fields decay inversely with the square of the distance, EEG signals are more sensitive to tissue anisotropies (Wolters et al., 2006), which may be larger in subjects with larger heads?

Finally, this study focused mainly on the underlying differences in gross morphology which may bias EEG results, but did not discuss when correcting for these differences may be necessary. Distance effects have been noted in several neurological disorders including increased head size in autism (Lainhart et al., 2006) which could lead to larger cortex-electrode distances, and cortical folding abnormalities in autism which lead to increased cortical depth vs typically developing controls (Nordahl et al., 2007). While the results presented here do not rule out amplitude as a useful marker of inter-subject differences in neural activity, we recommend caution when interpreting differences in scalp amplitude across subjects and populations. Ideally, cortical/head morphology would always be included as a co-variate when examining differences in non-invasive electrophysiological signal amplitude across populations. When such data (i.e. T1 images) are not available, source amplitude (obtained via solving the inverse problem) can partially account for these distance effects.

Conflicts of interest

The authors declare no competing financial interests.

Acknowledgements

This work was supported by the National Science and Engineering Council of Canada and the Canada Research Chair in Neurovascular Coupling.

Appendix A. Supplementary data

Supplementary data to this article can be found online at https://doi.org/10.1016/j.neuroimage.2019.03.010.

References

Ahlfors, S.P., Han, J., Lin, F.-H., Witzel, T., Belliveau, J.W., Hämäläinen, M.S., Halgren, E., 2010. Cancellation of EEG and MEG signals generated by extended and distributed sources. Hum. Brain Mapp. 31, 140–149. https://doi.org/10.1002/hbm.20851.

Bastos, A.M., Vezoli, J., Bosman, C.A., Schoffelen, J.-M., Oostenveld, R., Dowdall, J.R., De Weerd, P., Kennedy, H., Fries, P., 2014. Visual areas exert feedforward and feedback influences through distinct frequency channels. Neuron 85, 390–401. https://doi.org/10.1016/j.neuron.2014.12.018.

BRAINARD, D.H., 1997. The psychophysics toolbox. Spatial Vis. 10, 433–436.

Butler, R., Bernier, P.-M., Lefebvre, J., Gilbert, G., Whittingstall, K., 2017a. Decorrelated input dissociates narrow band γ power and BOLD in human visual cortex. J. Neurosci. 37.

Butler, R., Gilbert, G., Descoteaux, M., Bernier, P.-M., Whittingstall, K., 2017b. Application of polymer sensitive MRI sequence to localization of EEG electrodes. J. Neurosci. Methods 278, 36–45. https://doi.org/10.1016/j.jneumeth.2016.12.013.

Buzsáki, G., Anastassiou, C.A., Koch, C., 2012. The origin of extracellular fields and currents — EEG, ECoG, LFP and spikes. Nat. Rev. Neurosci. 13, 407–420. https://doi.org/10.1038/nrn3241.

Chamberland, M., Bernier, M., Fortin, D., Whittingstall, K., Descoteaux, M., 2015. 3D interactive tractography-informed resting-state fMRI connectivity. Front. Neurosci. 9, 275. https://doi.org/10.3389/fnins.2015.00275.

Cohen, D., Cuffin, B.N., Yunokuchi, K., Maniewski, R., Purcell, C., Cosgrove, G.R., Ives, J., Kennedy, J.G., Schomer, D.L., 1990. MEG versus EEG localization test using implanted sources in the human brain. Ann. Neurol. 28, 811–817. https://doi.org/10.1002/ana.410280613.

Cohen, M.X., 2017. Where does EEG come from and what does it mean? Trends Neurosci. 40, 208–218. https://doi.org/10.1016/j.tins.2017.02.004.

Coppola, G., Ambrosini, A., Clemente, L. Di, Magis, D., Fumal, A., Gérard, P., Pierelli, F., Schoenen, J., 2007. Interictal abnormalities of gamma band Activity in visual evoked responses in migraine: an indication of thalamocortical dysrhythmia? Cephalalgia 27, 1360–1367. https://doi.org/10.1111/j.1468-2982.2007.01466.x.

Cousijn, H., Haegens, S., Wallis, G., Near, J., Stokes, M.G., Harrison, P.J., Nobre, A.C., 2014. Resting GABA and glutamate concentrations do not predict visual gamma frequency or amplitude. Proc. Natl. Acad. Sci. Unit. States Am. 111, 9301–9306. https://doi.org/10.1073/pnas.1321072111.

Delorme, A., Makeig, S., 2004. EEGLAB: an open source toolbox for analysis of single-trial EEG dynamics including independent component analysis. J. Neurosci. Methods 134, 9–21. https://doi.org/10.1016/j.jneumeth.2003.10.009.

Deslauriers-Gauthier, S., Lina, J.-M., Butler, R., Bernier, P.-M., Whittingstall, K., Deriche, R., Descoteaux, M., 2017. Inference and Visualization of Information Flow in the Visual Pathway Using dMRI and EEG, Lecture Notes in Computer Science (Including Subseries Lecture Notes in Artificial Intelligence and Lecture Notes in Bioinformatics). https://doi.org/10.1007/978-3-319-66182-7_58.

Destexhe, A., Bedard, C., 2012. Do neurons generate monopolar current sources? J. Neurophysiol. 108, 953–955. https://doi.org/10.1152/jn.00357.2012.

Dickinson, A., Bruyns-Haylett, M., Jones, M., Milne, E., 2015. Increased peak gamma frequency in individuals with higher levels of autistic traits. Eur. J. Neurosci. 41, 1095–1101. https://doi.org/10.1111/ejn.12881.

Dickinson, A., Bruyns-Haylett, M., Smith, R., Jones, M., Milne, E., 2016. Superior orientation discrimination and increased peak gamma frequency in autism spectrum conditions. J. Abnorm. Psychol. 125, 412–422. https://doi.org/10.1037/abn0000148.

Evans, A.C., Janke, A.L., Collins, D.L., Baillet, S., 2012. Brain templates and atlases. Neuroimage 62, 911–922. https://doi.org/10.1016/j.neuroimage.2012.01.024.

Fries, P., Scheeringa, R., Oostenveld, R., 2008. Finding gamma. Neuron 58, 303–305. https://doi.org/10.1016/J.NEURON.2008.04.020.

Friston, K.J., Holmes, A.P., Worsley, K.J., Poline, J.-P., Frith, C.D., Frackowiak, R.S.J., 1994. Statistical parametric maps in functional imaging: a general linear approach. Hum. Brain Mapp. 2, 189–210. https://doi.org/10.1002/hbm.460020402.

Goense, J.B., Logothetis, N.K., 2008. Neurophysiology of the BOLD fMRI signal in awake monkeys. Curr. Biol. 18, 631–640. https://doi.org/S0960-9822(08)00442-9 [pii] 10.1016/j.cub.2008.03.054.

Gramfort, A., Papadopoulo, T., Olivi, E., Clerc, M., 2010. OpenMEEG: open source software for quasistatic bioelectromagnetics. Biomed. Eng. Online 9, 45. https://doi.org/10.1186/1475-925X-9-45.

Hari, R., Salmelin, R., 1997. Human cortical oscillations: a neuromagnetic view through the skull. Trends Neurosci. 20, 44–49. https://doi.org/10.1016/S0166-2236(96)10065-5.

Hermes, D., Miller, K.J., Wandell, B.A., Winawer, J., 2015a. Gamma oscillations in visual cortex: the stimulus matters. Trends Cognit. Sci. 19, 57–58. https://doi.org/10.1016/j.tics.2014.12.009.

Hermes, D., Miller, K.J., Wandell, B.A., Winawer, J., September 2015b. Stimulus dependence of gamma oscillations in human visual cortex. Cereb 25 (9), 2951–2959. https://doi.org/10.1093/cercor/bhu091.

Hillebrand, A., Barnes, G.R., 2002. A quantitative assessment of the sensitivity of whole-head MEG to activity in the adult human cortex. Neuroimage 16, 638–650.

Irimia, A., Van Horn, J.D., Halgren, E., 2012. Source cancellation profiles of electroencephalography and magnetoencephalography. Neuroimage 59, 2464–2474. https://doi.org/10.1016/j.neuroimage.2011.08.104.

Jenkinson, M., Beckmann, C.F., Behrens, T.E.J., Woolrich, M.W., Smith, S.M., 2012. FSL. Neuroimage 62, 782–790. https://doi.org/10.1016/j.neuroimage.2011.09.015.

Jia, X., Xing, D., Kohn, A., 2013. No consistent relationship between gamma power and peak frequency in macaque primary visual cortex. J. Neurosci. 33, 17–25. https://doi.org/10.1523/JNEUROSCI.1687-12.2013.

Kujala, J., Jung, J., Bouvard, S., Lecaignard, F., Lothe, A., Bouet, R., Ciumas, C., Ryvlin, P., Jerbi, K., 2015. Gamma oscillations in V1 are correlated with GABAA receptor density: a multi-modal MEG and Flumazenil-PET study. Sci. Rep. 5, 16347. https://doi.org/10.1038/srep16347.

Lainhart, J.E., Bigler, E.D., Bocian, M., Coon, H., Dinh, E., Dawson, G., Deutsch, C.K., Dunn, M., Estes, A., Tager-Flusberg, H., Folstein, S., Hepburn, S., Hyman, S., McMahon, W., Minshew, N., Munson, J., Osann, K., Ozonoff, S., Rodier, P., Rogers, S., Sigman, M., Spence, M.A., Stodgell, C.J., Volkmar, F., 2006. Head circumference and height in autism: a study by the collaborative program of excellence in autism. Am. J. Med. Genet. 140A, 2257–2274. https://doi.org/10.1002/ajmg.a.31465.

Lin, F.-H., Ahlfors, S.P., Witzel, T., Dale, A.M., Fischl, B.R., Liu, A.K., Belliveau, J.W., Halgren, E., n.d. Cancellation of MEG and EEG Signals with Distributed Source Activation on Realistic Cortical Surface.

Murakami, S., Okada, Y., 2006. Contributions of principal neocortical neurons to magnetoencephalography and electroencephalography signals. J. Physiol. 575, 925–936. https://doi.org/10.1113/jphysiol.2006.105379.

Musall, S., von Pföstl, V., Rauch, A., Logothetis, N.K., Whittingstall, K., 2014. Effects of neural synchrony on surface EEG. Cerebr. Cortex 24, 1045–1053. https://doi.org/10.1093/cercor/bhs389.

Muthukumaraswamy, S.D., 2013. High-frequency brain activity and muscle artifacts in MEG/EEG: a review and recommendations. Front. Hum. Neurosci. 7, 138. https://doi.org/10.3389/fnhum.2013.00138.

Muthukumaraswamy, S.D., Edden, R.A.E., Jones, D.K., Swettenham, J.B., Singh, K.D., 2009. Resting GABA concentration predicts peak gamma frequency and fMRI amplitude in response to visual stimulation in humans. Proc. Natl. Acad. Sci. Unit. States Am. 106, 8356–8361. https://doi.org/10.1073/pnas.0900728106.

Muthukumaraswamy, S.D., Singh, K.D., Swettenham, J.B., Jones, D.K., 2010. Visual gamma oscillations and evoked responses: variability, repeatability and structural MRI correlates. Neuroimage 49, 3349–3357. https://doi.org/10.1016/j.neuroimage.2009.11.045.

Nordahl, C.W., Dierker, D., Mostafavi, I., Schumann, C.M., Rivera, S.M., Amaral, D.G., Van Essen, D.C., 2007. Cortical folding abnormalities in autism revealed by surface-based morphometry. J. Neurosci. 27, 11725–11735. https://doi.org/10.1523/JNEUROSCI.0777-07.2007.

Nunez, P.L., Srinivasan, R., 2006. Electric Fields of the Brain: the Neurophysics of EEG. Oxford University Press.

Peiker, I., David, N., Schneider, T.R., Nolte, G., Schöttle, D., Engel, A.K., 2015. Perceptual integration deficits in autism spectrum disorders are associated with reduced interhemispheric gamma-band coherence. J. Neurosci. 35.

Provencher, D., Hennebelle, M., Cunnane, S.C., Bérubé-Lauzière, Y., Whittingstall, K., 2016. Cortical thinning in healthy aging correlates with larger motor-evoked EEG desynchronization. Front. Aging Neurosci. 8, 63. https://doi.org/10.3389/fnagi.2016.00063.

Riera, J.J., Ogawa, T., Goto, T., Sumiyoshi, A., Nonaka, H., Evans, A., Miyakawa, H., Kawashima, R., 2012. Pitfalls in the dipolar model for the neocortical EEG sources. J. Neurophysiol. 108, 956–975. https://doi.org/10.1152/jn.00098.2011.

Robson, S.E., Muthukumarawswamy, S.D., John Evans, C., Shaw, A., Brealy, J., Davis, B., McNamara, G., Perry, G., Singh, K.D., 2015. Structural and neurochemical correlates of individual differences in gamma frequency oscillations in human visual cortex. J. Anat. 227, 409–417. https://doi.org/10.1111/joa.12339.

Schwarzkopf, D.S., Robertson, D.J., Song, C., Barnes, G.R., Rees, G., 2012. The frequency of visually induced gamma-band oscillations depends on the size of early human visual cortex. J. Neurosci. 32, 1507–1512. https://doi.org/10.1523/JNEUROSCI.4771-11.2012.

Shaw, A.D., Moran, R.J., Muthukumaraswamy, S.D., Brealy, J., Linden, D.E., Friston, K.J., Singh, K.D., 2017. Neurophysiologically-informed markers of individual variability and pharmacological manipulation of human cortical gamma. Neuroimage 161, 19–31. https://doi.org/10.1016/J.NEUROIMAGE.2017.08.034.

Simon, D.M., Wallace, M.T., 2016. Dysfunction of sensory oscillations in autism spectrum disorder. Neurosci. Biobehav. Rev. 68, 848–861. https://doi.org/10.1016/j.neubiorev.2016.07.016.

Spencer, K.M., Niznikiewicz, M.A., Shenton, M.E., McCarley, R.W., 2008. Sensory-Evoked gamma oscillations in chronic schizophrenia. Biol. Psychiatry 63, 744–747. https://doi.org/10.1016/j.biopsych.2007.10.017.

Sun, L., Grützner, C., Bölte, S., Wibral, M., Tozman, T., Schlitt, S., Poustka, F., Singer, W., Freitag, C.M., Uhlhaas, P.J., 2012. Impaired gamma-band Activity during perceptual organization in adults with autism spectrum disorders: evidence for dysfunctional network activity in frontal-posterior cortices. J. Neurosci. 32.

Tadel, F., Baillet, S., Mosher, J.C., Pantazis, D., Leahy, R.M., 2011. Brainstorm: a user-friendly application for MEG/EEG analysis. Comput. Intell. Neurosci. 2011, 879716. https://doi.org/10.1155/2011/879716.

Tan, H.-R.M., Lana, L., Uhlhaas, P.J., 2013. High-frequency neural oscillations and visual processing deficits in schizophrenia. Front. Psychol. 4, 621. https://doi.org/10.3389/fpsyg.2013.00621.

van Pelt, S., Boomsma, D.I., Fries, P., 2012. Magnetoencephalography in twins reveals a strong genetic determination of the peak frequency of visually induced gamma-band synchronization. J. Neurosci. 32, 3388–3392. https://doi.org/10.1523/JNEUROSCI.5592-11.2012.

van Pelt, S., Shumskaya, E., Fries, P., 2018. Cortical volume and sex influence visual gamma. Neuroimage 178, 702–712. https://doi.org/10.1016/J.NEUROIMAGE.2018.06.005.

Whittingstall, K., Stroink, G., Gates, L., Connolly, J., Finley, A., 2003. Effects of dipole position, orientation and noise on the accuracy of EEG source localization. Biomed. Eng. Online 2, 14. https://doi.org/10.1186/1475-925X-2-14.

Wolters, C.H., Anwander, A., Tricoche, X., Weinstein, D., Koch, M.A., MacLeod, R.S., 2006. Influence of tissue conductivity anisotropy on EEG/MEG field and return current computation in a realistic head model: a simulation and visualization study using high-resolution finite element modeling. Neuroimage 30, 813–826. https://doi.org/10.1016/J.NEUROIMAGE.2005.10.014.